Experimental study of the novel tuned mass damper with inerter which enables changes of inertance

P. Brzeski[a], M. Lazarek[a], P. Perlikowski[a,*]

[a]*Division of Dynamics, Lodz University of Technology, Stefanowskiego 1/15, 90-924 Lodz, Poland*

Abstract

In this paper we present the experimental verification of the novel tuned mass damper which enables changes of inertance. Characteristic feature of the proposed device is the presence of special type of inerter. This inerter incorporates a continuously variable transmission that enables stepless changes of inertance. Thus, it enables to adjust the parameters of the damping device to the current forcing characteristic. In the paper we present and describe the experimental rig that consists of the massive main oscillator forced kinematically and the prototype of the investigated damper. We perform a series of dedicated experiments to characterize the device and asses its damping efficiency. Moreover, we perform numerical simulations using the simple mathematical model of investigated system. Comparing the numerical results and the experimental data we legitimize the model and demonstrate the capabilities of the investigated tuned mass damper. Presented results prove that the concept of the novel type of tuned mass damper can be realized and enable to confirm its main advantages. Investigated prototype device offers excellent damping efficiency in a wide range of forcing frequencies.

Keywords: Inerter, damping, tuned mass damper, prototype, experimental investigation

1. Introduction

Tuned mass dampers (TMD) are widely used for damping of unwanted oscillations of mechanical and structural systems. The first record of TMD-like device can be found in the work by Watts [1] published in 1883. In 1909 Frahm described and patented the classic TMD [2]. His device is extremely effective in reducing the response of the damped structure only in the principal resonance. Den Hartog proposed to add a viscous damper to Frahm's system design [3] to expand its range of effectiveness. Thanks to that simple modification, the TMD can reduce vibrations of the main body in wide range of excitation frequencies around the principal resonance. Another way to broaden the range of TMD's effectiveness was proposed by Roberstson [4] and Arnold [5] who interchange

*Corresponding author
Email address: przemyslaw.perlikowski@p.lodz.pl (P. Perlikowski)

the linear spring of TMD by the nonlinear one (with the linear and nonlinear parts of stiffness). Recently there are many papers considering new or modified designs and applications of TMDs [6, 7, 8, 9, 10]

This paper is devoted to the examination of a novel design of TMD introduced in our previous publication [11]. Essence of the concept lies in the special type of an inerter. Initially inerters [12] were successfully applied in sports cars' suspensions [13, 14]. Now we observe growing number of studies on other possible applications: in railway vehicles' suspensions [15, 16], devices that absorb impact forces [17] or protect buildings from earthquakes [18, 19]. In [20] authors study the influence of the inerter on the natural frequencies of vibration systems while in [21] we find the review of the effects of an inerter on the tuned mass absorber.

In a very new papers [22, 23, 24, 25, 26] one can find the idea of usage of the inerter as a part of the TMD. Numerical results prove that optimally designed TMD with inerter outperforms classical TMDs. Still, to work efficiently, all considered devices have to be precisely tuned which can be hard to achieve or even impossible in some cases. Moreover proposed TMDs with inerters suffer from susceptibility to detuning. The above problems may be eliminated using the device equipped with an inerter that enables stepless and accurate changes of inertance that we proposed in 2014 [11]. The idea of inertance-changeable inerters was also considered for different applications by Chen et al. [27, 28, 29]. In [11] we prove that such a property can be achieved by using a continuously variable transmission (CVT) with gear-ratio control system. In [11] we describe the possible realization of the TMD that incorporates inertance-changeable inerter. Then, we perform numerical analysis of its properties. In this paper, we present the experimental investigation of the existing prototype of the device.

Although the mathematical model of the inerter is very simple its practical realizations do not follow the model strictly. It is mainly caused by factors like: internal motion's resistances, friction, play in gears and etc. Most of these effects are modelled using nonlinear functions that are much more complex than the formula proposed by Smith et. al. In our recently published paper [30] we present the analysis of the inerter nonlinearities on the performance of the TMD.

Aforementioned phenomena influence the response of the structure and the efficiency of a TMD. That is why in this paper we describes a series of experiments of prototype TMD performed on a unique experimental rig. Then, we compare experimental data with numerical results to legitimize the mathematical model of the examined TMD.

The paper is organized as follows. In Section 2 we present the idea that lies behind the examined TMD. Section 3 contains the description of the experimental rig and in Section 4 we present its physical and mathematical models. In Section 5 we present the data collected during the experimental tests of the prototype and compare it to results obtained from the numerical model. In Section 6 we summarize our results.

2. The idea behind the examined TMD design

The classical TMD introduced by Frahm [2] consists of mass on a linear spring. Such a device is extremely effective in suppressing oscillations of the main structure for the frequency equal to the natural frequency of the TMD. For the frequencies outside small range around its main resonance it increases the amplitude of the system's motion. Because of this disadvantage, the classical TMD has extremely small range of effectiveness and is hardly ever used. We can extend the range of effectiveness by adding a viscous damper, using a nonlinear spring instead of linear one etc. Still, the increase in the range of effective damping impairs damping properties in principal resonance (when vibrations frequency is equal to the natural frequency of the TMD). Therefore, we always have to face a tradeoff between the most effective mitigation of vibrations for given frequency or achieving the tolerable damping properties in a wide range of vibration frequencies. This problem can be minimized by novel types of TMDs which incorporates inerters or magnetorheological dampers that are intensively developed nowadays. Unfortunately, all of the devices are not as efficient as classical TMD for its tuned frequency.

The solution for the problems would be the TMD with as small damping as permissible (to secure best possible damping efficiency for natural frequency of the device) and controllable natural frequency. In our previous paper [11] we propose the new design of a TMD that meets both of these requirements. The device we propose is schematically presented in Fig. 1. It consist of inertial component (A) that is coupled via elastic link (B), inerter (C), and dashpot (D) to damped structure (E). The essential part of the proposed TMD design is the special type on an inerter (C). This inerter contains the CVT that allows stepless adjustments of the inertia it brings to the system. In our previous paper we present detailed description of the concept, sample construction layout of the TMD, its mathematical model and numerical investigation of achievable damping efficiency.

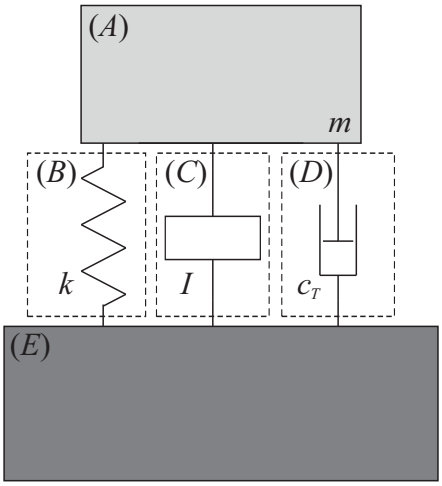

Figure 1: Scheme of the proposed TMD model.

Current inertance of the inerter (C) is given by parameter I. Inertial element (A) is described by parameter m and parameter k is used to characterize the stiffness of the spring (B). Parameters m and k have constant values while the value of parameter I can be modified as it depends on the current transmission ratio. We introduce a dashpot (D) to model damping that is always present in the system due to internal damping, friction and motion resistance introduced by the presence of the CVT [31, 32]. Dashpot (D) is described by damping coefficient c_T. We assume that c_T has relatively small value and does not influence the natural frequency of the considered TMD. Hence, to calculate the natural frequency of the considered TMD we can use the following formula:

$$\omega_{TMD}(I) = \sqrt{\frac{k}{m+I}} \tag{1}$$

Thanks to the presence of the CVT we are able to steplessly control the inertia that is brought to the system by the inerter. This in turn means that we can adjust the inertance value I and control the natural frequency of vibrations of the TMD $\omega_{TMD}(I)$. In consequence, the examined device can be easily tuned to the current excitation frequency to mitigate unwanted motion more effectively. Therefore, by introducing an inerter with the CVT we are able to increase TMD's damping efficiency and the range of effectiveness. Numerical results presented in [11] prove that the proposed TMD offers improvement over other known TMDs. Apart from the above, the proposed device is easy to tune and can be re-tuned when the circumstances change. In this paper we present an experimental investigation of the prototype TMD which is schematically presented in Fig. 1.

3. Model of the considered system

Now we describe the physical and the mathematical model of the experimental rig (description of the rig is presented in the next Section). In Fig. 2 we show two schematic diagrams that refer

to the analysed model. In the subplot (a) we present the detailed model which corresponds to the experimental rig and shows all important parts of the device which influence values' of parameters of the system while in the subplot (b) we show simplified model with reduced number of parameters.

Both models have two degrees of freedom and consist of two coupled oscillators that can move in the vertical direction. The first one serves as a model of the main oscillator which motion we are going to mitigate. It is connected with the support and forced via kinematic excitation. The second oscillator is connected to the first one and represents the TMD. It is connected with the main oscillator via linear spring, viscous damper, inerter and element that models dry friction.

The motion of the system is described by two generalized coordinates: the position of the main oscillator by coordinate x, while the displacement of the TMD by coordinate y. The main oscillator is characterized with the following parameters: M is its mass, $6K$ is the stiffness of the single spring that connects the main mass to the ground and C is the viscous damping coefficient of dashpot that links mass M and the support. Formula $A\cos\left(\frac{s\pi}{30}t\right)$ expresses the kinematic excitation of the main oscillator with the frequency $\frac{s\pi}{30}$ that corresponds to the speed $s\,[rpm]$ of the forcing servomotor and the crank on the exciting plate set to A. During the investigation we analyse the response of the structure for fixed crank $A = 0.02955\,[\mathrm{m}]$ and different frequencies of excitation that corresponds to the following range of rotational speeds $s\epsilon\,\langle 150,\,250\rangle$ [rpm].

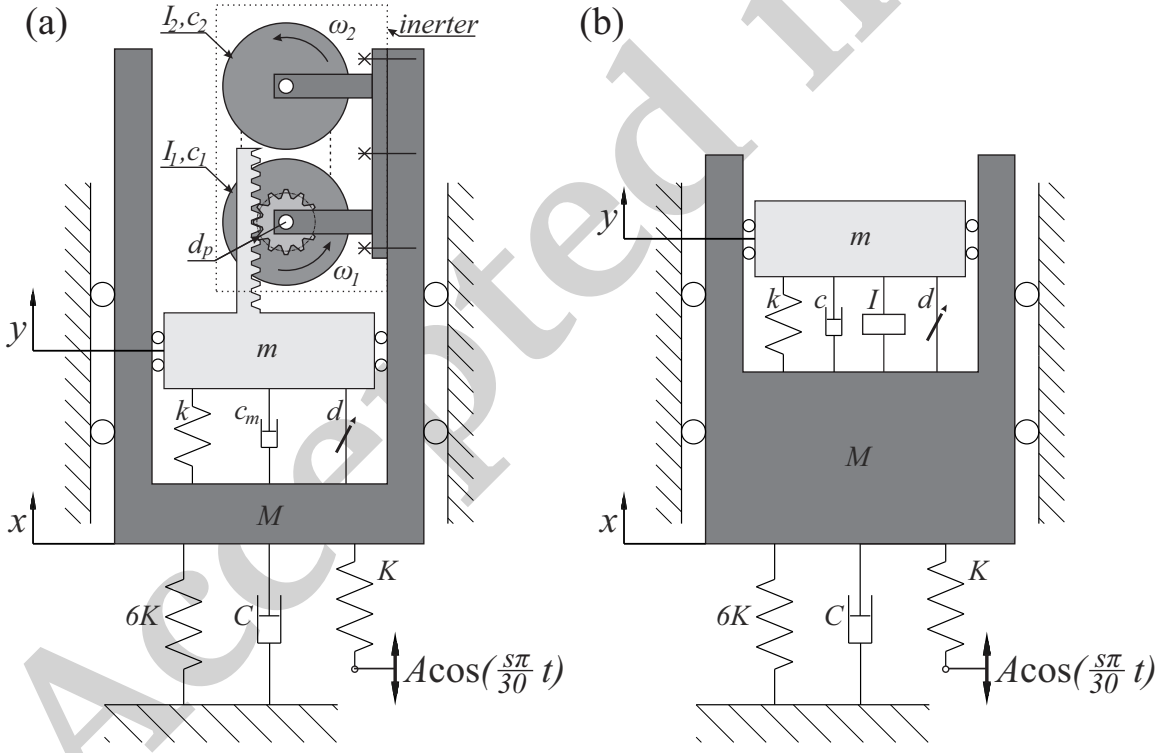

Figure 2: Physical models of the system and notation of parameters with different level of details and parameters.

In subplot (a) we also present the model of the TMD with comprehensive presentation of the inerter model. To characterize this system we use the following parameters values: the moving mass is given by m, the stiffness of the spring that connects it to the main oscillator is described with parameter k . The viscous damping coefficient of the dashpot that connect mass m with M is given byc_m while d is the amplitude of dry friction force that is generated between the interacting parts. The pitch diameter of the pinion that cooperates with the moving rack is given by d_p; the inertia of the drive shaft of the CVT is given by I_1 and its rotational speed is described as ω_1. For the driven shaft that is combined with the flywheel we use I_2 and ω_2 respectively. We assume that the motion of each shaft of the CVT is damped with the torque proportional to its velocity. Damping coefficients are given by parameter c_1 and c_2 for the drive and driven shaft respectively. Parameter r is the current ratio of the CVT.

The values of the parameters has been measured in a series of dedicated experiments. After that we further tuned the values of parameters using curve fitting methods to adjust the model of the examined rig. Appointed values of parameters are the following: $M = 102.66\,[\mathrm{kg}]$, $K = 8181.0\,[\frac{\mathrm{N}}{\mathrm{m}}]$, $C = 20.0\,[\frac{\mathrm{Ns}}{\mathrm{m}}]$, $A = 0.02955\,[\mathrm{m}]$, $m = 11.26\,[\mathrm{kg}]$, $k = 10448.0\,[\frac{\mathrm{N}}{\mathrm{m}}]$ (that equals to the equivalent stiffness of the four springs used in the rig), $c_m = 15.2\,[\frac{\mathrm{Ns}}{\mathrm{m}}]$, $c_1 = 0.00439\,[\mathrm{Nms}]$ $c_2 = 0.00375\,[\mathrm{Nms}]$, $d = 11.0\,[\mathrm{N}]$, $d_p = 0.06\,[\mathrm{m}]$, $I_1 = 0.00572\,[\mathrm{kgm}^2]$, $I_2 = 0.01046\,[\mathrm{kgm}^2]$, $r\epsilon\,\langle 0.5283,\, 1.893\rangle\ [-]$.

Before we derive the equations of motion of the system presented in Fig. 2 (a) we introduce some relations between the introduced parameters and coordinates. The rotational speeds of the CVT shafts can be calculated using the following formulas:

$$\omega_1 = \frac{\dot{y} - \dot{x}}{d_p}, \tag{2}$$

$$\omega_2 = r\omega_1. \tag{3}$$

The total kinetic energy T, and potential energy V and Rayleigh dissipation function D of the considered system are given by the following formulas:

$$T = \frac{1}{2}M\dot{x}^2 + \frac{1}{2}m\dot{y}^2 + \frac{1}{2}I_1\dot{\omega}_1^2 + \frac{1}{2}I_2\dot{\omega}_2^2, \tag{4}$$

$$V = \frac{1}{2}6Kx^2 + \frac{1}{2}K\left(x - A\cos\left(\frac{s\pi}{60}t\right)\right)^2 + \frac{1}{2}k\left(y - x\right)^2, \tag{5}$$

$$D = \frac{1}{2}C\dot{x}^2 + \frac{1}{2}c_m\left(\dot{y} - \dot{x}\right)^2 + \frac{1}{2}c_1{\omega_1}^2 + \frac{1}{2}c_2{\omega_2}^2. \tag{6}$$

Apart from the above we use a continuous model of dry friction and assume that the force generated in the the dry friction element is given as:

$$d\frac{2}{\pi}\arctan\left(10^5(\dot{x} - \dot{y})\right). \tag{7}$$

Using the Lagrange equations of the second kind we reach the equations of motion of the system presented in Fig. 2(a). After simplification the equations of motion can be written as follows:

$$\begin{gathered} M\ddot{x}+7Kx+C\dot{x}+\left(\frac{1}{d_p^2}I_1+\frac{r^2}{d_p^2}I_2\right)(\ddot{x}-\ddot{y})+k\,(x-y)+ \\ +\left(c_m+\frac{1}{d_p^2}c_1+\frac{r^2}{d_p^2}c_2\right)(\dot{x}-\dot{y})+d\frac{2}{\pi}\arctan\left(10^5(\dot{x}-\dot{y})\right)=KA\cos\left(\frac{s\pi}{30}t\right) \end{gathered}, \tag{8}$$

$$m\ddot{y}-\left(\frac{1}{d_p^2}I_1+\frac{r}{d_p^2}I_2\right)(\ddot{x}-\ddot{y})-k\,(x-y)-\left(c_m+\frac{1}{d_p^2}c_1+\frac{r^2}{d_p^2}c_2\right)(\dot{x}-\dot{y})-d\frac{2}{\pi}\arctan\left(10^5(\dot{x}-\dot{y})\right)=0. \tag{9}$$

To reduce the number of parameters and to simplify our model we propose the system that is presented in 2(b). Now we use simplified model of the inerter that is described only with the inertance I. Apart from the model contains single dashpot with varying damping coefficient $c(I) = c_{const} + c_I I$. Thanks to these changes we interchange parameters I_1, I_2, c_m, c_1 c_2, d_p, r with only two parameters that are defined as follows:

$$I=\frac{1}{d_p^2}I_1+\frac{r^2}{d_p^2}I_2. \tag{10}$$

$$c(I)=c_m+\frac{1}{d_p^2}c_1+\frac{r^2}{d_p^2}c_2=c_{const}+c_I I. \tag{11}$$

Assuming the accessible range of the CVT ratios we calculate the range in which we can smoothly change parameter $I\epsilon\,\langle 2.4,\,12.0\rangle$. Then, we calculate the values of constant and varying part of viscous damping coefficient receiving: $c_{const} = 16.15\,[\frac{\mathrm{Ns}}{\mathrm{m}}]$ and $c_I = 0.3583\,[\frac{\mathrm{Ns}}{\mathrm{mkg}}]$ respectively. The behaviour of simplified model is governed by the following equations of motion:

$$M\ddot{x}+7Kx+C\dot{x}+I\,(\ddot{x}-\ddot{y})+k\,(x-y)+c(I)\,(\dot{x}-\dot{y})+d\frac{2}{\pi}\arctan\left(10^5(\dot{x}-\dot{y})\right)=KA\cos\left(\frac{s\pi}{30}t\right), \tag{12}$$

$$m\ddot{y}-I\,(\ddot{x}-\ddot{y})-k\,(x-y)-c(I)\,(\dot{x}-\dot{y})-d\frac{2}{\pi}\arctan\left(10^5(\dot{x}-\dot{y})\right)=0. \tag{13}$$

In the numerical analysis we use Eqs (12,13) for sake of simplicity. It is important to notice that the simplified mathematical model that we reach after reducing the number of parameters is almost exactly the same as in the model from our previous article in which we introduce the novel TMD design [11]. There are only two minor differences. The first is the addition of dry friction element and the second is the varying damping coefficient of the dashpot that connects TMD to the damped mass. These changes were introduced to improve the agreement between the results of numerical simulations and data collected during experiments. Nevertheless, both models give results that are similar qualitatively and quantitatively.

4. Experimental rig

In this section we describe the the experimental rig presented it in Fig. 3. Two panels correspond to general view of the rig and zoom of the inerter respectively. The experimental rig consists of one degree of freedom kinematically forced oscillator and the prototype TMD. The frames of the main mass and the TMD are made from aluminium and steel profiles. The outer steel structure No. 1 has a square base of $\square 0.7$ [m] and is 1.6 [m] tall. It supports main inner structure (part Nos. 2(a,b)) suspended with main springs (part No. 3) and kinematic excitation assembly (part No. 4). The main mass structure (part No 5) is made from aluminium profiles.It can move in vertical direction and our aim is to mitigate this motion. Vertical guiding of the main mass is realized using the linear bearings which slides on four vertical shafts positioned in the corners (one of them is marked as part No. 6) . The main mass assembly (with mass M) supports the CVT and the flywheel of the TMD (parts in frame No. 7).

The moving part of the TMD (part No. 8) with mass m is guided through the system of rollers (part No. 9) and performs vertical movement relative to the main mass assembly restricted by a four TMD's springs (one of them is marked as a part No. 10). Vertical movement is converted to rotational motion by the gear rack (part No. 11) connected to a gear (part No 12). The CVT presented in Fig. 3(b)) consists of the drive shaft (part No. 13), the flywheel (part No. 14) and the driven shaft (part No. 15). Kinematic forcing is realized with the Panasonic MINAS A5 servomotor connected to the crank mechanism. Excitation is transmitted by the spring (part No. 16) with the same stiffness as springs supporting the main structure. The servomotor posses 1.5 [kW] of nominal power and 7.16 [Nm] of nominal torque. The servomotor is controlled by Panasonic FP-X C30 PLC controller. Such configuration enables to change servo rotational speed with the accuracy of 1.0 [rpm] which corresponds to 0.105 [rad/s] and 0.0167 [Hz] (assuming the accuracy of three significant figures).

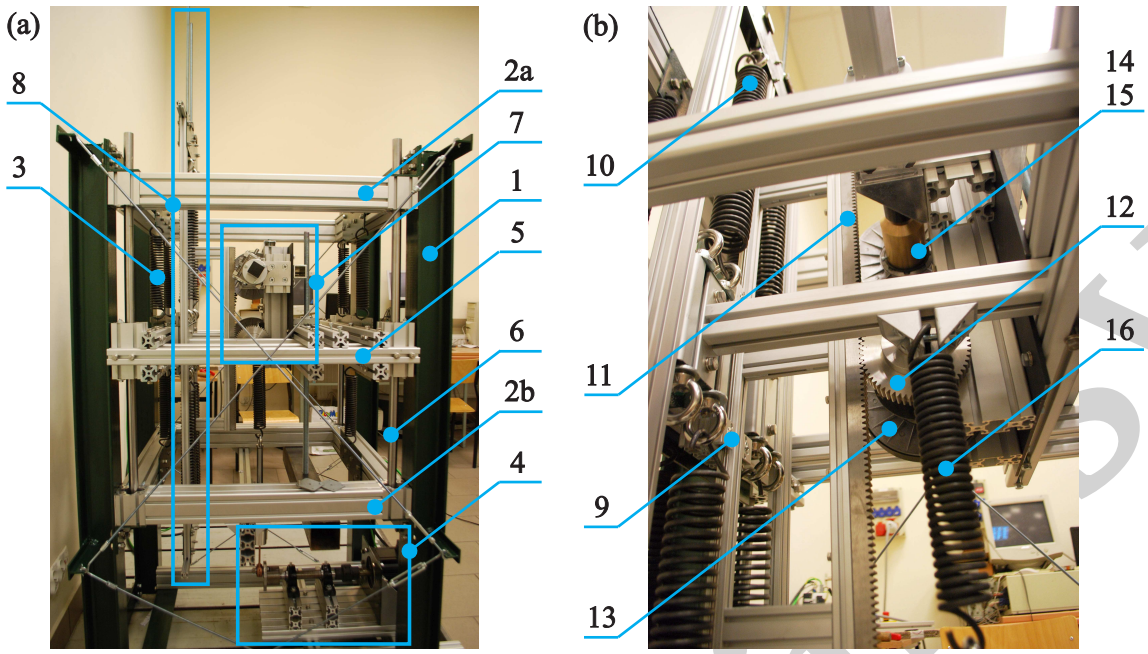

Figure 3: Realization of the laboratory rig with the prototype TMD: (a) general view and (b) detailed view of the TMD.

5. Comparison between numerical results and experimental data

In this section we present and compare the results of numerical simulations with the data collected during experiments. We focus on the frequency response curve (FRC) of the main oscillator. Such approach enables us to present a large number of data in single plot which gives good overview of both damping efficiency of the TMD and its range of effectiveness. We start with the investigation of the structure without TMD. Then we analyze the system with the damper for six equally spaced settings of the CVT which refers to six different values of I parameter. Finally, to present the overall capabilities of the damping device we merge the results obtained for different settings of the CVT. This enables us to prove the advantages that comes from the usage of the CVT.

5.1. Sensors and data acquisition system

Data acquisition system allows us to detect the position of the main mass and the crank. We use a precise laser sensor Microepsilon optoNCDT1302 with 0.2 [m] range to measure the main mass position. Another laser sensor Keyence LK-G157/LK-G152 together with the dedicated controller LK-GD500 is used for detecting the crank position. We also measure the velocities of the main mass and the TMD with two Polytec HSV 700 sensor heads controlled by two Polytec HSV2002 controllers. All signals are acquired through the Bruel & Kjaer frame type 3660 equipped with Bruel & Kjaer 3050 channel input module. Such configuration allows us to acquire six high-precision

inputs with an input frequency up to 51.2 [kHz]. All signals are collected using the Pulse LabShop software and further exported to Mathematica software for processing of the data.

5.2. Response of the structure without the TMD

At the beginning we analyse the response of the main oscillator without the TMD. We performed a series of measurements for 26 different rotational speeds of the forcing servomotor. The points are not uniformly distributed over the whole analysed range of frequencies. It is because around the resonant frequency (3.75 [Hz] = 225 [rpm]) the amplitude of the structure exceeds the limitations of the rig. That is why we omit the range $s\epsilon\,\langle 221,\,230\rangle$ [rpm]. Also for the frequencies that are far from the resonance peak we record fewer points as the amplitude of the structure barely changes in that range. For each considered speed of the forcing servomotor we record the time trace of the main mass after we reach an attractor. Then we read its amplitude of motion. This gives us a single point for the plot. In Fig. 4 we present the comparison between the results of experiments and numerical simulations. The dots corresponds to the experimental data while the lines were obtained from the numerical model using the continuation of periodic solutions (AUTO-07p software [33]). When we consider only the motion of the main oscillator (case without TMD) our mathematical model presented in Section 3 can be simplified to one equation that is the following:

$$M\ddot{x} + 7Kx + C\dot{x} = KA\cos\left(\frac{s\pi}{30}t\right), \tag{14}$$

In Fig. 4 (a) we present the whole FRC while in subplot (b) we show the magnification of the curve which corresponds to the amplitude that is reachable on the experimental rig. While the subplot (a) gives us the overall insight about the systems dynamics subplot (b) enables to asses the agreement between the experiment and simulations.

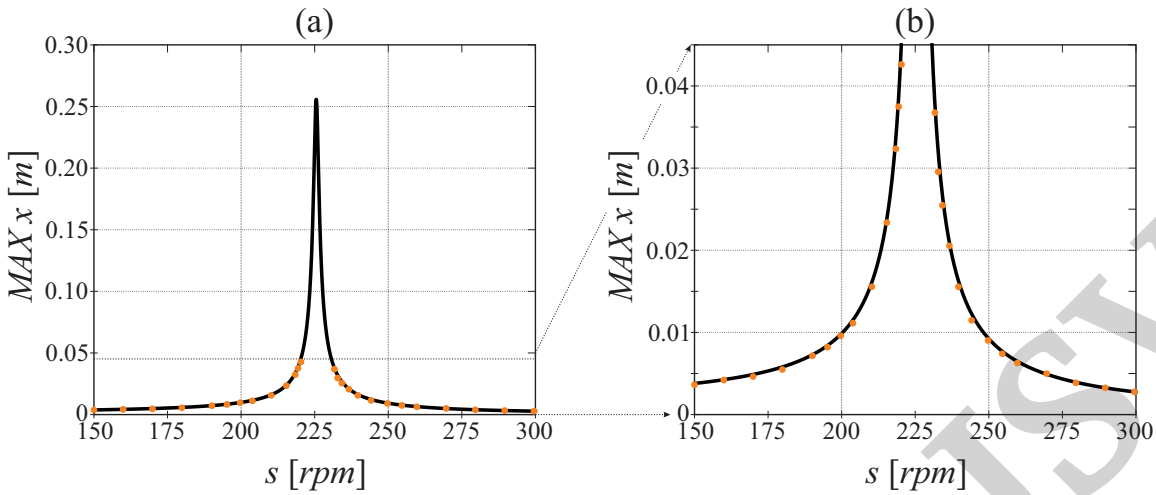

Figure 4: FRCs of the base oscillator without TMD. Continuous lines have been obtained via numerical continuation while the dots corresponds to experimental data. Subplot (a) presents the full FRC while in subplot (b) we show zoom of the range that is accessible on the experimental rig.

Analysing Fig. 4 we can say that the main oscillator has relatively small damping. In fact, the appointed value of viscous damping coefficient refers to 0.4% of critical damping. That is why the resonance peak is abrupt and in in the resonance we observe extremely large amplitude of motion that is far from what can be achieved on the rig. Still, in subplot (b) we see that all of the dots are in a good agreement with the line which legitimize the model and obtained parameters values.

5.3. Structure with the TMD

After analysing the response of the structure without the TMD we couple the device and examine its damping properties. The TMD that we use incorporates the CVT that enables to tune its parameters to the current forcing frequency. Therefore, to present its capabilities we could just present the response of the structure assuming that the ratio of the CVT is always adjusted to the current excitation. This will be done in the next subsection while now we want to give an overview of the dynamics of the system with the device. For that purpose we pick six equally spaced ratios of the CVT that refers to six different values of I parameter, namely 2.4, 4.2, 5.2, 7.2, 9.3, 12.0 [kg]. Then, for each setting we obtain FRC of the main oscillator numerically and experimentally (using the procedure described in the previous subsection). This gives us six FRCs that are presented in Fig. 5.

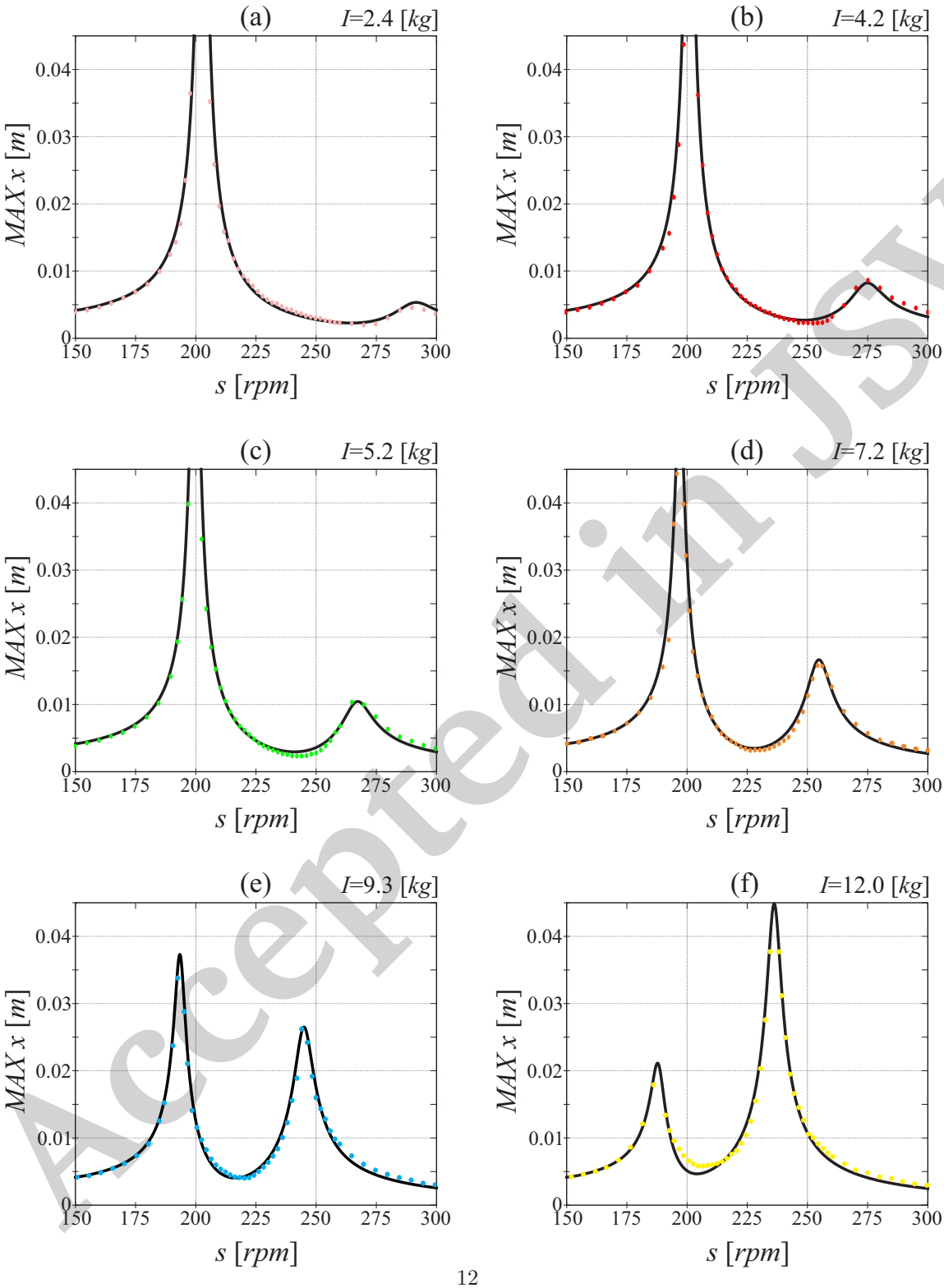

Figure 5: FRCs of the base oscillator with TMD obtained for six different settings of the CVT. Above each subplot (a) we give the value of I for which the curve was calculated. Continuous lines have been obtained via numerical continuation while the dots correspond to the experimental data.

In Fig. 5 continuous lines presents the result of numerical simulations and dots are the points obtained experimentally. Above each subplot we indicate the value of parameter I that was used. Analysing the presented results we can say that in general results of simulations are in very good agreement with experimental data. There are some points which diverge from the lines but we have remember that we use really simple linear model that does not take into account many aspects of the experimental rig such as for example backlash in rack and pinion gear or the elasticity of the CVT belt. Overall divergence is so small that it can also be caused by some inherent noise. In our previous publication [11] we prove that both parametric and additive noise can cause some minor changes in the shape of FRC. Nevertheless, presented results legitimize the model and prove that it enables to reproduce dynamical phenomena observed in the experimental rig.

5.4. Overall damping efficiency

Analysing the data presented in Fig. 5 we can say that the most important point on each subplot is the minimum along the FRC. It is, because the minimum corresponds to the frequency of excitation for which we used the optimized CVT setting. Thanks to the CVT we can create infinite number of similar FRCs. It is a big advantage because we can always adjust the gear ratio to achieve the minimum amplitude. Therefore to fully present the capabilities of the proposed TMD design we connect their minima. By that we recieve curves that demonstrate the amplitude of the main mass under presence of the TMD with changeable inertnace. In Fig. 6 we show the overall damping efficiency of the TMD and compare FRC for the system without the TMD and the amplitude curves for the system with the TMD.

In 6(a) we present the result of numerical simulations. We merge six FRCs presented in Fig. 5 and add the red dashed line. This line represents the overall damping efficiency of the TMD. It received by connecting the minima of 200 FRCs calculated for equally spaced values of parameter I taken from the accessible range $I \in \langle 2.4, 12 \rangle$ [m].

In 6(b) we overlap all points recorded during the experiments with the TMD. Then we create a blue line by connecting the minima of experimentally obtained FRCs. This line presents the actual damping efficiency of the prototype TMD device that we tested. In Fig. 6(c) we compare lines from subplots (a) and (b) with the FRCs of the main oscillator without the TMD. We see that we are able to significantly reduce the motion of the structure in the whole considered range. Using the proposed TMD we can reduce the amplitude up to 71 times in the resonance (from 0.256 [m] to 0.0036 [m]). Still around the resonance peak we preserve the impressive level of reduction: 10 times for $s = 220$ [rpm] (from 0.044 [m] to 0.0043 [m]) and 14 times for $s = 230$ [rpm] (from 0.051 [m] to 0.0036 [m]).

To enable better comparison between numerical simulations and experimental data in Fig. 6(d) we present the magnification of subplot (c). We see that results from simulations and the tests of the prototype are in good agreement. Both approaches enable to prove the concept of novel TMD design and show its main advantages such as wide range of effectiveness and impressive reduction of the damped structure amplitude of motion.

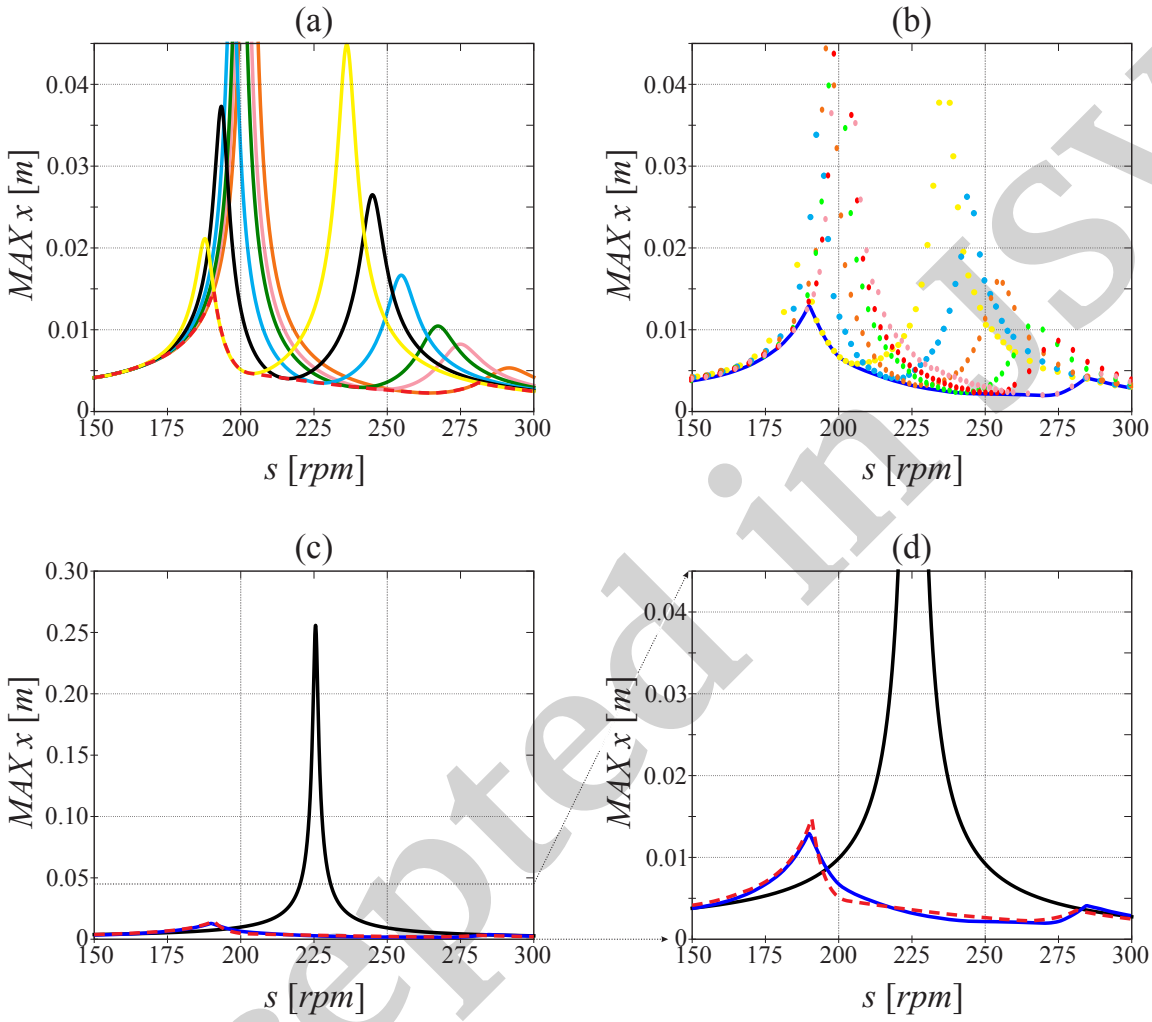

Figure 6: Amplitude curves presenting the overall damping efficiency of the TMD with changeable inertance. Results from numerical simulations (a) and experimental data (b) are compared to the response of the structure without the device (c,d). Continuous lines have been obtained via numerical continuation while the dots corresponds to experimental data.

Analysing the amplitude of the structure with the TMD (Fig. 6 (a,b)) we see that for $s\epsilon$ (175, 200) [rpm] we still observe some significant increase of the amplitude of motion. This unwanted property can be easily eliminated by increasing the accessible CVT ratios or by adjusting the values of the CVT parameters (I_1, I_2, d_p). In Fig. 7 we present the enhance in the damping efficiency that can be achieved by only increasing the maximum CVT ratio by 31%. Such an increase enables to broaden the accessible range of I values to 19.5 [kg].

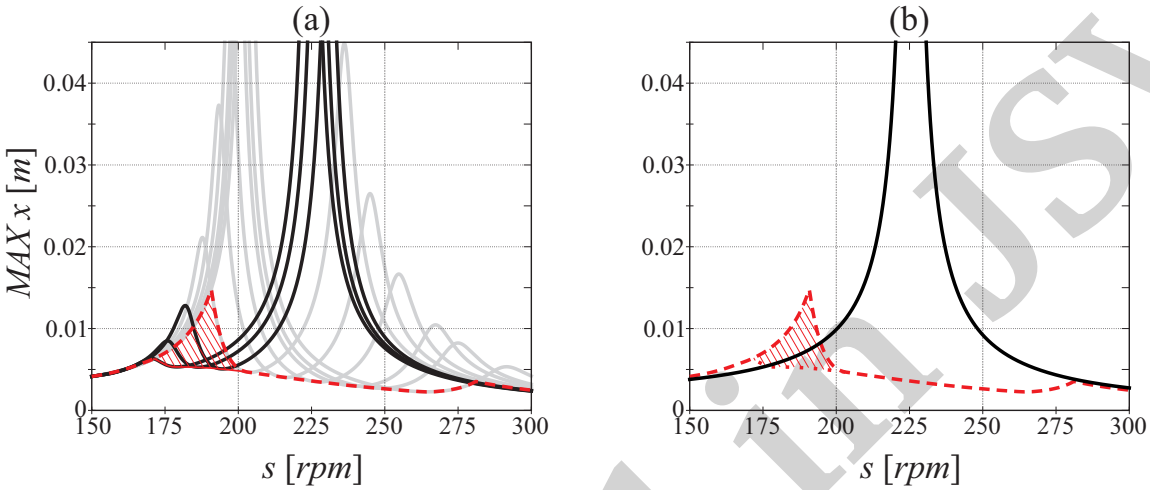

Figure 7: Improvement in the damping efficiency that can be achieved by increasing the maximum CVT ratio by 31%. Black lines were calculated for enabled values of I parameter. Dotted line present the amplitude of the main mass under the presence of the improved TMD design. Hatched areas shows the gain in the amplitude reduction.

In Fig. 7(a) we use grey lines to present the FRCs from Fig. 6(a). We complement the plot with the black lines that were calculated numerically for following values of inertance: $I = 14.5$ [kg], $I = 17.0$ [kg] and $I = 19.5$ [kg]. By connecting the minima of FRCs the new amplitude curve is created and marked as a red dotted line. This line presents the overall improvement of the TMD efficiency and hatched area shows the gain over the existing prototype. In Fig. 7 (b) we compare the FRC for the structure without the TMD with the amplitude curve for the system with the device that has broadened range of accessible I values.

Comparison of the dashed and dotted red lines let us claim that with small modification we are able to significantly reduce the response of the structure for $s\epsilon$ (175, 200) [rpm]. The range of the considered TMD effectiveness can also be enhanced by using a multiple stage CVT or a transmission with accelerating gears only. In our next paper we will consider different constructions of CVTs and compare them to find their strengths and weaknesses. Nevertheless, presented results prove that by a small change in the construction of the CVT we are able to further increase the range of the TMD effectiveness and achieve outstanding damping efficiency for extremely wide range of excitation frequencies.

Results presented in this section prove that the examined TMD design offers impressive damping efficiency in a notably wide range of excitation frequencies. Currently, we are finishing the design of an active control of the CVT ratio. This will allow to automatically adjust the inertance value depending on the measured frequency of vibrations. The control algorithm that we are developing will enhance the advantages of the TMD and make it particularly effective in relation to the structures that are forced with varying frequencies. In our upcoming paper we analyse different active control algorithms and compare them to point out their advantages and limitations.

6. Conclusions

In this paper we present the experimental investigation of the prototype of the novel TMD design [11]. The essential part of the investigated device is a special type of an inerter that includes a continuously variable transmission. We use the experimental rig that enables to examine the response of the structure without the TMD and with the tested device. Then, we compare the experimental data with numerical simulations to assess the modeling approach and examine the damping efficiency of the prototype.

We start experimental tests by analysing the response of the structure without the TMD. Due to limitations of the rig we are not able to obtain the full frequency response of the structure. Nevertheless, we record enough points to legitimize the mathematical model of the main oscillator and its parameters values. Then, we attach the prototype TMD and perform a series of experimental tests. For six equally spaced settings of the CVT we obtain FRCs of the damped structure. Experimental data are in perfect agreement with numerical results and enable to prove the concept of the new TMD design. Apart from that, we obtain (both experimentally and numerically) the overall amplitude curve that present the response of the structure with the TMD that has optimized the CVT's gear ratio to the current forcing frequency.

Presented results prove that the examined prototype of the TMD with the inerter and the CVT provides remarkable damping properties in a notably wide range of vibration frequencies. Moreover, the properties of the considered TMD can be reproduced with simple mathematical model which does not require large computational effort. This allow us to claim that the proposed TMD design is robust and can be applied in many different areas.

Acknowledgement

This work is funded by the Polish Ministry of Science and Higher Education, Iuventus Plus programme, Project No. 0352/ IP2/2015/73. PB is supported by the Foundation for Polish Science (FNP) under the framework of "Start" fellowship.

Supplementary Material

In supplementary material we add two videos that are showing the performance of our rig before and after the resonance frequency of the main body (217 [rpm] and 235 [rpm]).

References

[1] P. Watts, On a method of reducing the rolling of ships at sea, *Transactions of the Institute of Naval Architects* 24 (1883) 165–190.

[2] H. Frahm, Device for damping vibrations of bodies, US Patent US 989958 A, 1909.

[3] J. P Den Hartog, *Mechanical Vibrations*, McGraw-Hill, New York, 1934.

[4] R. E. Roberson, Synthesis of a nonlinear dynamic vibration absorber, *Journal of Franklin Institute* 254 (1952) 205–220.

[5] F. R. Arnold, Steady-state behavior of systems provided with nonlinear dynamic vibration absorbers, *Journal of Applied Mathematics* 22 (1955) 487–492.

[6] A. Dall'Asta, L. Ragni, A. Zona, L. Nardini, W. Salvatore, Design and experimental analysis of an externally prestressed steel and concrete footbridge equipped with vibration mitigation devices, *Journal of Bridge Engineering* 21(8) (2016).

[7] L. Li, G. Song, M. Singla, Y.-L. Mo, Vibration control of a traffic signal pole using a pounding tuned mass damper with viscoelastic materials (ii): experimental verification, *Journal of Vibration and Control* 21(4) (2015) 670–675.

[8] J. G. Johnson, C. P. Pantelides, and L. D. Reaveley, Nonlinear rooftop tuned mass damper frame for the seismic retrofit of buildings, *Earthquake Engineering & Structural Dynamics* 44(2) (2015) 299–316.

[9] Y. Yang, W. Dai, and Q. Liu, Design and implementation of two-degree-of-freedom tuned mass damper in milling vibration mitigation, *Journal of Sound and Vibration* 335 (2015) 78–88.

[10] F. Tubino and G. Piccardo, Tuned mass damper optimization for the mitigation of human-induced vibrations of pedestrian bridges, *Meccanica* 50(3) (2015) 809–824.

[11] P. Brzeski, T. Kapitaniak, and P. Perlikowski, Novel type of tuned mass damper with inerter which enables changes of inertance, *Journal of Sound and Vibration* 349 (2015) 56–66.

[12] M.C. Smith, Synthesis of mechanical networks: the inerter, *Automatic Control, IEEE Transactions on* 47(10) (2002) 1648–1662.

[13] F.-C. Wang M. C. Smith. Performance benefits in passive vehicle suspensions employing inerters, *Proceedings of the IEEE Conference on Decision and Control* 3 (2004) 2258–2263.

[14] M.Z.Q. Chen, C. Papageorgiou, F. Scheibe, Fu cheng Wang, and M.C. Smith, The missing mechanical circuit element, *Circuits and Systems Magazine, IEEE* 9(1) (2009) 10–26.

[15] F.-C. Wang and M.-K. Liao, The lateral stability of train suspension systems employing inerters, *Vehicle System Dynamics* 48(5) (2010) 619–643.

[16] F.-C. Wang, M.-R. Hsieh, and H.-J. Chen, Stability and performance analysis of a full-train system with inerters, *Vehicle System Dynamics* 50(4) (2012) 545–571.

[17] R. Faraj, J. Holnicki-Szulc, L. Knap, and J. Senko, Adaptive inertial shock-absorber, *Smart Materials and Structures* 25(3) (2016) 035031.

[18] I. Takewaki, S. Murakami, S. Yoshitomi, and M. Tsuji, Fundamental mechanism of earthquake response reduction in building structures with inertial dampers, *Structural Control and Health Monitoring* 19(6) (2012) 590–608.

[19] Y.-C. Chen, J.-Y. Tu, and F.-C. Wang, Earthquake vibration control for buildings with inerter networks, In *Control Conference (ECC), 2015 European*, 3137–3142, July 2015.

[20] M.Z.Q. Chen, Y. Hu, L. Huang, and G. Chen, Influence of inerter on natural frequencies of vibration systems, *Journal of Sound and Vibration* 333(7) (2013) 1874–1887.

[21] P. Brzeski, E. Pavlovskaia, T. Kapitaniak, and P. Perlikowski, The application of inerter in tuned mass absorber. *International Journal of Non-Linear Mechanics* 70 (2015) 20–29.

[22] M. Zilletti, Feedback control unit with an inerter proof-mass electrodynamic actuator, *Journal of Sound and Vibration* 369 (2016) 16–28.

[23] I. F. Lazar, S.A. Neild, and D.J. Wagg, Using an inerter-based device for structural vibration suppression, *Earthquake Engineering & Structural Dynamics* 43(8) (2014) 1129–1147.

[24] L. Marian and A. Giaralis, Optimal design of a novel tuned mass-damper-inerter (tmdi) passive vibration control configuration for stochastically support-excited structural systems, *Probabilistic Engineering Mechanics* 38 (2014) 156–164.

[25] S. Krenk and J. Høgsberg, Tuned resonant mass or inerter-based absorbers: unified calibration with quasi-dynamic flexibility and inertia correction, *Proceedings of the Royal Society of London A: Mathematical, Physical and Engineering Sciences* 472(2185) (2016) 20150718.

[26] Y. Hu, M.Z.Q. Chen, Performance evaluation for inerter-based dynamic vibration absorbers, *International Journal of Mechanical Sciences* 99 (2015) 297-307.

[27] MZ. Chen, Y. Hu, C. Li, G. Chen. Semi-active suspension with semi-active inerter and semi-active damper, *IFAC World Congress 2014, Cape Town, South Africa* 19(1) (2014) 11225-11230.

[28] Y. Hu, M.Z.Q. Chen, S. Xu, Y. Liu, Semiactive Inerter and Its Application in Adaptive Tuned Vibration Absorbers, *IEEE Transactions on Control Systems Technology* 25(1) (2017) 294-300.

[29] M. Z. Chen, Y. Hu, C. Li, G. Chen, Application of semi-active inerter in semi-active suspensions via force tracking, *Journal of Vibration and Acoustics* 138(4) (2016) 041014.

[30] P. Brzeski and P. Perlikowski, Effects of play and inerter nonlinearities on the performance of tuned mass damper, *Nonlinear Dynamics* (2016) doi:10.1007/s11071-016-3292-1.

[31] B.F. Feeny and J.W. Liang. A decrement method for the simultaneous estimation of coulomb and viscous friction. *Journal of Sound and Vibration* 195(1) (1996) 149–154.

[32] M. Wiercigroch B. Horton and X. Xu, Transient tumbling chaos and damping identification for parametric pendulum, *Philosophical Transactions of the Royal Society of London, A*, 366 (2007) 767–784.

[33] E. J. Doedel, *AUTO-07P: Continuation and bifurcation software for ordinary differential equations*, Montreal, Canada, April 2006.